J. Fluid Mech. (2025), *vol.* 1014, R3, doi:10.1017/jfm.2025.10219



Thickness model for viscous impinging liquid sheets

Ziyang Peng[1], **Xuan Liu**[1], **Zhuo-Yang Song**[1], **Bo Wang**[2], **Zhengxuan Cao**[3], **Erjun Wu**[2], **Jiarui Zhao**[1], **Ying Gao**[1], **Xiaodong Chen**[1] **and Wenjun Ma**[1,4,5]

[1]State Key Laboratory of Nuclear Physics and Technology, School of Physics, Peking University, Beijing 100871, PR China

[2]School of Aerospace Engineering, Beijing Institute of Technology, Beijing 100081, PR China

[3]National Key Laboratory of Shock Wave and Detonation Physics, Institute of Fluid Physics China, Academy of Engineering Physics, Mianyang, PR China

[4]Beijing Laser Acceleration Innovation Center, Huairou, Beijing 101400, PR China

[5]Guangdong Institute of Laser Plasma Accelerator Technology, Guangzhou 510080, PR China

Corresponding authors: Wenjun Ma, wenjun.ma@pku.edu.cn; Ziyang Peng, pengjiang_123@stu.pku.edu.cn; Xiaodong Chen, xiaodong.chen@bit.edu.cn

(Received 5 March 2025; revised 5 April 2025; accepted 1 May 2025)

Ultra-thin liquid sheets generated by impinging two liquid jets are crucial high-repetition-rate targets for laser ion acceleration and ultra-fast physics, and serve widely as barrier-free samples for structural biochemistry. The impact of liquid viscosity on sheet thickness should be comprehended fully to exploit its potential. Here, we demonstrate experimentally that viscosity significantly influences thickness distribution, while surface tension primarily governs shape. We propose a thickness model based on momentum exchange and mass transport within the radial flow, which agrees well with the experiments. These results provide deeper insights into the behaviour of liquid sheets and enable accurate thickness control for various applications, including atomization nozzles and laser-driven particle sources.

Key words: thin films, jets, low-dimensional models

1. Introduction

Free-flowing liquid sheets formed by impinging two identical jets at a certain point have been observed and studied for more than 190 years (Savart 1833). They are used widely in industry, with applications including fuel atomization in rocket engines (Oefelein & Yang 1993), synthesis of nanoparticles (Baber *et al.* 2016) and drug and bio-materials delivery

© The Author(s), 2025. Published by Cambridge University Press.

https://doi.org/10.1017/jfm.2025.10219 Published online by Cambridge University Press

(Visser *et al.* 2018). In recent years, liquid sheets have also been employed in fundamental research as ultra-thin and barrier-free targets, such as detecting ultra-fast processes in liquids (Loh *et al.* 2020) and generating particles and radiation by interaction with ultra-intense lasers (Morrison *et al.* 2018; Tcypkin *et al.* 2019; Kim *et al.* 2023; Knight *et al.* 2024). The thickness of the liquid sheet is a key factor for these studies and technologies. For instance, it determines the size of the drops after sheet breakup in impinging jets atomizers (Majumdar & Tirumkudulu 2018). The energies of laser-accelerated ions rely strongly on the thickness of the targets (Macchi *et al.* 2013): protons up to 150 MeV have been generated by exploiting 200–300 nm ultra-thin foils (Ziegler *et al.* 2024). Sub-micrometre-thick samples are also essential for applications in soft X-ray, infrared (IR) and photoelectron spectroscopy (Woo *et al.* 2018; Yang *et al.* 2021; Stemer *et al.* 2023). In all these applications, precise prediction and control of liquid-sheet thickness over a wide range of parameters are essential.

Many theories have been developed to predict the thickness of impinging sheets (Taylor 1961; Hasson & Peck 1964; Ibrahim & Przekwas 1991; Choo & Kang 2001; Bush & Hasha 2004; Bremond & Villermaux 2006; Li & Ashgriz 2006; Xiaodong & Vigor 2019). Among these, the Hasson and Peck (H&P) model (Hasson & Peck 1964), assuming a uniform velocity within the liquid sheet, predicts that the thickness distribution depends only on the impinging angle, jet diameter and the polar coordinates relative to the impinging point. The model has been validated by many experiments and has become an essential foundation for theories and applications (Panao & Delgado 2013; Ekimova *et al.* 2015; Sanjay & Das 2017; Zhang *et al.* 2021; Buttersack *et al.* 2023; Füle *et al.* 2024). However, it overlooks the effects of liquid viscosity, a significant factor yet poorly understood. Numerical simulations indicate that the thickness of the sheet increases and becomes more uniform as the viscosity increases (Lu & Corvalan 2014). Theories suggest that thickness decreases as the Reynolds number increases, but there is still a lack of experimental verification and quantitative analysis (Yang *et al.* 2014). The expanding requirements of microscale liquid sheets and the growing diversity of liquids employed render viscous effects increasingly significant, highlighting the need for further research to unveil fully how liquid properties, particularly viscosity and surface tension, influence liquid-sheet thickness (Peng *et al.* 2024; Streeter *et al.* 2025).

In principle, the influence of liquid properties can be identified experimentally by independently regulating viscosity or surface tension and accurately measuring the sheet's thickness. However, this is challenging in practice, as viscosity and surface tension are inherent properties of liquids, not independently adjustable parameters. Another challenge lies in the lack of precise measurements for the two-dimensional (2-D) thickness distribution of the liquid sheet, likely stemming from limitations in measurement accuracy.

In this work, we explore the effects of viscosity on the thickness of impinging liquid sheets by carefully controlling their physical properties and measuring the sheet thickness with nanometre-level precision. Three types of liquids with distinctly different viscosities and surface tensions are mixed as the test samples, which allows independent control of these parameters in a wide range. We observe that viscosity exerts a dominant influence on the thickness, while surface tension affects the shape of liquid sheets. Based on 2-D Navier–Stokes equations and reasonable approximation, we propose a thickness model for ultra-thin impinging liquid sheets, which agrees well with experimental results. The model reveals the underlying physics of viscous effects, enabling more accurate thickness predictions. Using this model, we demonstrate the dynamic capability to control the thickness of the liquid sheet.

https://doi.org/10.1017/jfm.2025.10219 Published online by Cambridge University Press

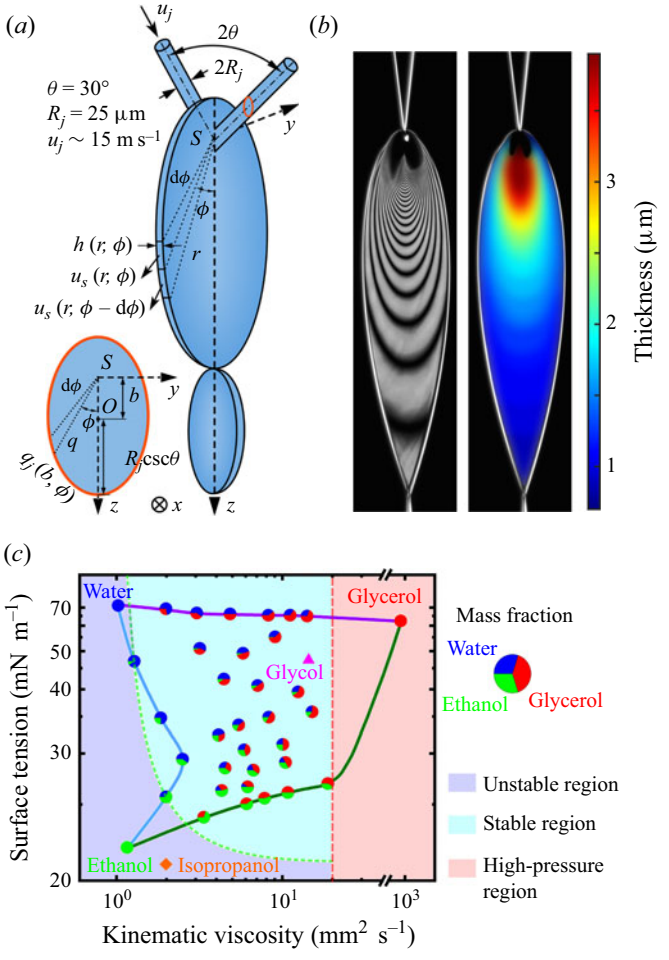


Figure 1. (*a*) Schematic of the liquid-sheet generation. The ellipse with the red edge is a jet cross-section. (*b*) Interference fringes and the retrieved thickness distribution. (*c*) Phase diagram of kinematic viscosity and surface tension of the ternary liquid mixtures in the experiment. The pie charts show the mass composition of the mixtures.

2. Results and discussion

Figure 1(*a*) shows the generation process of an impinging liquid sheet: two identical cylindrical jets with a diameter of $R_j = 25$ μm, ejected from capillaries, impinge at $2\theta = 60°$ and form a leaf-like sheet in the orthogonal direction. The high jet velocities ($u_j \sim 20$ m s^{-1}) render the effects of gravity negligible. We measure the absolute thickness at specific points via white-light reflection spectrum, while the relative thickness distribution can be determined through the interference fringes of monochromatic, as illustrated in figure 1(*b*). The accuracy of this novel technique is 0.5 %, and the spatial resolution is 5 μm (Peng *et al.* 2024).

To differentiate the effects of viscosity and surface tension, we blend three liquids – water, ethanol and glycerol – to create a mixed solution. Figure 1(*c*) shows the phase diagram of these mixtures, where the small pie charts depict the mass proportions of each constituent liquid. Numerous experiments indicate that the diagram can be divided into three regions. In the high-pressure region, highly viscous mixtures

https://doi.org/10.1017/jfm.2025.10219 Published online by Cambridge University Press

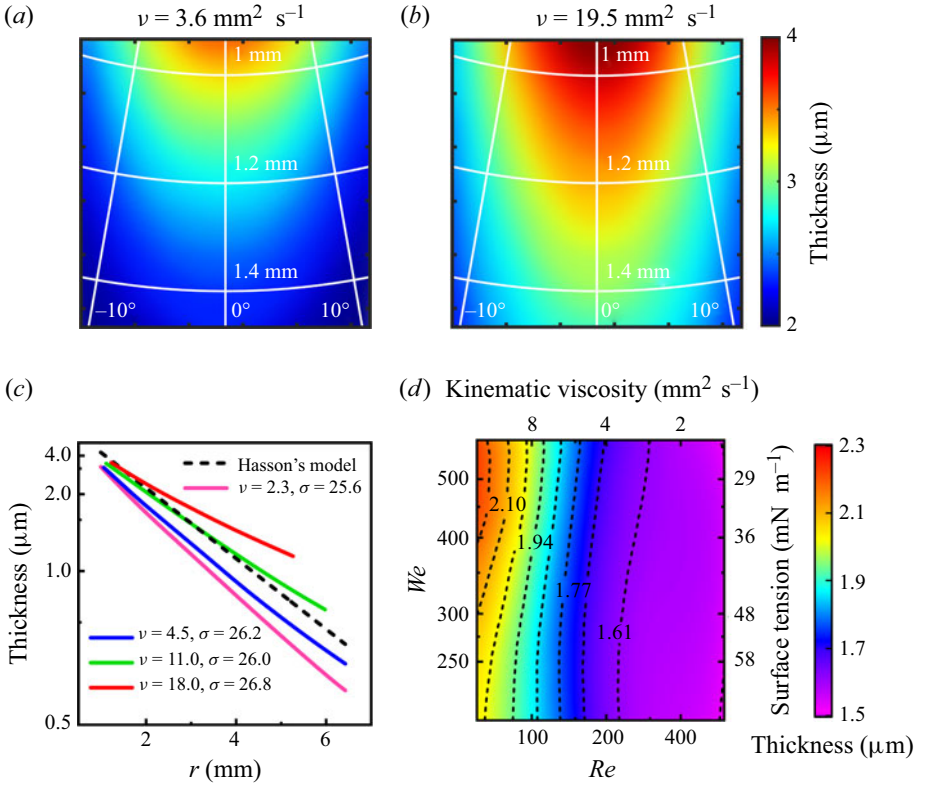


Figure 2. (*a*,*b*) Thickness distribution of two mixtures with $\nu = 3.6$ mm^2 s^{-1} and $\nu = 19.5$ mm^2 s^{-1}, respectively. (*c*) Thickness along the z-axis for mixtures with similar surface tension but different kinematic viscosity. (*d*) Thickness a fixed point on the z-axis as a function of Reynolds number and Weber number. The flow rate of a single jet is held constant at 2 mL min^{-1} for all data presented in figure 2.

can cause excessive pressure that exceeds the fluid system's capacity. In the unstable region, the mixtures have low viscosity or high surface tension. The unbalance between viscous damping and surface-tension restoration results in unstable sheets, consistent with previous findings (Bush & Hasha 2004; Sanjay & Das 2017). Consequently, most of the mixtures investigated in this work are in the stable region, where exceptionally stable liquid-sheet chains form. All data are measured at a temperature of 24.4 to 24.8 °C.

Figures 2(*a*) and 2(*b*) shows the measured thickness distribution of two mixtures with kinematic viscosity of $\nu = 3.6$ mm^2 s^{-1} and $\nu = 19.5$ mm^2 s^{-1}, respectively. Their surface tensions are similar ($\sigma = 25 \pm 1$ mN m^{-1}), and all other parameters are identical. The thickness decreases with distance r but increases with viscosity at a given position, especially along the z-axis. The separation point S is the origin (Hasson & Peck 1964), and the z-axis is 0°. The thickness discrepancy between the two is approximately 30 % at $\phi = 0°$ azimuth, decreasing to less than 10 % at $\phi = 10°$ azimuth. Such a trend was observed widely in the experiments. We plot the thickness h along the z-axis in figure 2(*c*) for four other mixtures with similar surface tension but different kinematic viscosity. One can see the thicknesses for all the mixtures are nearly identical at small r, and become smaller with the increase of r. The mixtures with higher viscosity are significantly thicker at given r, which is beyond the prediction of the H&P model. We found that $h \propto r^{-0.86}$ for $\nu = 11.0$, and $h \propto r^{-0.97}$ for $\nu = 2.3$, while the H&P model (Hasson & Peck 1964) states

https://doi.org/10.1017/jfm.2025.10219 Published online by Cambridge University Press

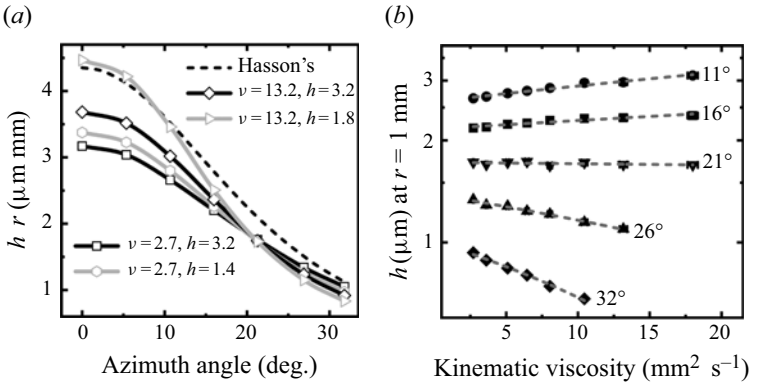


Figure 3. (*a*) The thickness–distance product hr as a function of azimuth angle. The thickness of each curve is fixed. (*b*) Thickness at $r = 1$ mm for different azimuth angles. The dashed line represents the predictions of our model presented in this work.

that the thickness follows $h \propto r^{-1}$ (dashed line in figure 2*c*):

$$hr = R_j^2 \sin^3\theta/(1 - \cos\phi\cos\theta)^2. \tag{2.1}$$

While the viscosity profoundly affects the thickness of the sheets, the surface tension exhibits negligible influence. We use Reynolds number ($Re = 2R_j u_j/\nu$) and Weber number ($We = 2\rho R_j {u_j}^2/\sigma$), ρ is density of the liquid in figure 2(*d*) to illustrate the thickness at $r = 2$ mm on the z-axis. The gradient of the iso-thickness line is determined mainly by viscosity, represented by Re, with surface tension, represented by We, having a relatively minor impact. Surface tension acts primarily on the rim of the liquid sheets, affecting their overall shape, but its effects on thickness will be disregarded in the subsequent discussion.

The liquid viscosity not only affects the variation of thickness with r but also significantly influences its dependence on the azimuth angle ϕ. Figure 3(*a*) presents experimental results for two mixtures with $\nu = 2.7$ mm^2 s^{-1} and $\nu = 13.2$ mm^2 s^{-1} at different ϕ. Beyond the prediction of the H&P model, experimental results indicate a complex dependence of the thickness–distance product hr on ϕ for mixtures with different viscosity. At 0°, curves with greater thickness are positioned above curves with smaller thickness; however, this trend reverses approximately at 21°. This indicates that the thickness decreases more rapidly than r^{-1}, resulting in thinner sheets at large azimuth angles, a phenomenon not previously observed (Choo & Kang 2001; Lu & Corvalan 2014; Yang *et al.* 2014). With r fixed at 1 mm , we show this azimuth-dependent viscosity effect in figure 3(*b*). Viscosity affects sheet thickness oppositely around 21°, consistent with the trends shown in figure 3(*a*), resulting in a steeper gradient, with thicker sheets at small angles and thinner sheets at large angles. The thickness characteristics of these viscous liquid sheets may benefit applications such as laser ion acceleration (Chen *et al.* 2009).

To further understand these angle-dependent viscous effects, we develop a theoretical model that describes the thickness distribution by considering momentum exchange and mass transport resulting from viscous interactions between adjacent radial regions. We assume a steady flow of the ultra-thin liquid sheet, neglecting gravity, evaporation, air friction and x-direction velocity. The coordinate system and the elliptical cross-section of the impinging jet follows figure 1(*a*). After impingement, the flow forms a radial velocity field originating from the separation point S . For inviscid liquids,

https://doi.org/10.1017/jfm.2025.10219 Published online by Cambridge University Press

this radial field is maintained as the sheet evolves, allowing mass conservation to be $2\sin\theta \mathrm{d}\phi \int_0^{q_j(\phi)} q u_j \mathrm{d}q = u_s h r \mathrm{d}\phi$, where u_j and u_s are the velocities in the jet and the sheet, respectively. The distance between S and the jet boundary q_j is

$$q_j(\phi) = \left\{ b\cos\phi\sin^2\theta + \left[R_j^2\left(1-\cos^2\phi\cos^2\theta\right) - b^2\sin^2\phi\sin^2\theta\right]^{1/2}\right\} \Big/ \left(1-\cos^2\phi\cos^2\theta\right). \tag{2.2}$$

Here the parameter b is the distance of S to the central point of the jet, as shown in figure 1(a). It determines the initial flow distribution from the jet to the sheet. For the subsequent analysis, a constant u_j over the whole cross-section is assumed, yielding $hr = q_j^2 \sin\theta u_j/u_s$. We experimentally ensure this assumption by setting a sufficiently long pre-impinging length (free jet length before impinging), which is also validated by OpenFOAM simulations (see supplementary material).

In the H&P model, it is assumed that u_s equals u_j everywhere, thus leading to $b = R_j\cot\theta$ and (2.1). However, u_s is actually non-uniform (Choo & Kang 2002), and deviates from a purely radial pattern for viscous liquids. With a perturbative treatment of viscous effects, u_s is a sum of zeroth- and first-order terms: $\boldsymbol{u}_s = (u + u_r^{(1)})\boldsymbol{e}_r + u_\phi^{(1)}\boldsymbol{e}_\phi$. Under this assumption, it can be proved from the 2-D Navier–Stokes equations that $u = u(\phi)$ is independent of r, and $u_\phi^{(1)}(r,\phi) = 2\nu\partial u/ur\partial\phi\ln(r/R)$ increases monotonously with the azimuth angle from zero. The angle-dependent $u(\phi)$ signifies a direct viscosity-driven momentum exchange in adjacent radial regions, while the presence of angular velocity $u_\phi^{(1)}$ implies mass transport across these regions. With this understanding of u_s, we can add a perturbation term to $hr = {q_j}^2\sin\theta[1+\delta(r,\phi)]$. The equation governing δ is derived by applying this with the flow conservation equation and the Navier–Stokes equations (see supplementary material). The results reveal a weak dependence of $\partial\delta/\partial r$ on r : $\partial\delta/\partial r \propto a(\phi)[1+o(r,\phi)]$, validated experimentally as shown in figure 4(a). In the first-order approximation, we neglect the higher-order terms of δ with respect to r and get an elegant thickness model:

$$h = \frac{q_j^2(\phi)\sin\theta}{r}\left[1 + a(\phi)\frac{\nu r}{Q}\right]. \tag{2.3}$$

Here Q is the jet flow rate, and the dimensionless viscous coefficient $a(\phi)$ is a function of u/u_j. This model exhibits a remarkably simple structure: the thickness varies as $1/r$ plus a constant $a(\phi)\nu/Q$ at any given azimuth. Consequently, with all other factors fixed, altering the liquid viscosity causes a proportional change in thickness at any position. In contrast to the H&P model, $h = {q_j}^2\sin\theta/r$, $a(\phi)$ describes the angular distribution of the viscous effects, while ν, r and Q determine their strength. The physics of $\delta = a(\phi)\nu r/Q$ is clear: larger r indicate more complete momentum and mass exchange, leading to stronger viscous effects; larger Q values, conversely, correspond to shorter interaction times and thus weaker viscous effects.

Since δ is proportional to r, figure 4(b) shows the slope of δ with r at various flow rates and azimuth angles, using the form $h = h_0(1+kr)$. With ϕ and Q fixed, k is proportional to the viscosity, and this proportionality is inversely proportional to the flow rate. These results support $\delta \propto \nu r/Q$ described by our model in (2.3).

Another important aspect is the determination of $a(\phi)$, which describes the angular distribution of momentum exchange and mass transport. It depends on the zeroth-order

https://doi.org/10.1017/jfm.2025.10219 Published online by Cambridge University Press

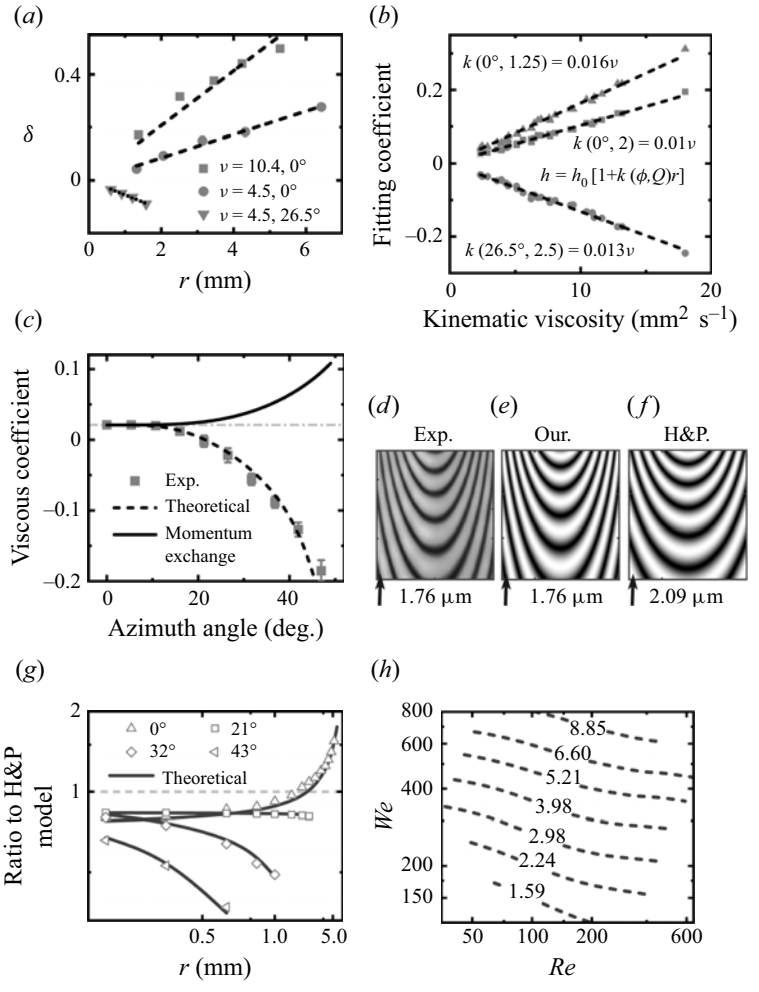


Figure 4. (*a*) The proportional relationship between thickness deviation δ and r. (*b*) Linear fitting of the slope of $\partial\delta/\partial r$ with respect to ν. The units of Q are mLmin^{-1}. (*c*) Angular distribution of the viscous coefficient $a(\phi)$. (*d*) Measured interference fringes of a mixture with $\nu = 18.0$. (*e*,*f*) Interference fringes predicted by our model and by the H&P model, respectively. (*g*) The experimental results compared with our model and the H&P model. (*h*) The length of liquid sheets (mm) as a function of Re and We.

radial velocity $u(\phi)$ and the angular velocity $u_\phi^{(1)}(r, \phi)$. Indeed, $u_\phi^{(1)}$ is also a function of $u(\phi)$. Given the symmetry and periodicity of $u(\phi)$, we can employ a cosine series expansion to investigate its form: $u = u_j \sum_k a_k \cos(k\phi)$, ak refers to the expansion coefficients at each level of trigonometric expansion. $u(\varphi)$ depends on q_j and the conservation equations of mass, momentum and energy from the jet to the sheet. Generally, b can be expressed as $b = \beta R_j \cot\theta$ (Choo & Kang 2007). Our experimental data yield a best-fit value of $\beta = 0.69$, and obtain

$$u/u_j = 0.147 + 0.408\cos\phi + 0.879\cos 2\phi \\ -0.767\cos 3\phi + 0.186\cos 4\phi. \tag{2.4}$$

Equation (2.4) demonstrates universal applicability at $\beta = 0.69$, i.e. the impinging angle $\theta = 30°$. Figure 4(*c*) shows the theoretical value of $a(\phi)$ (dashed line) and experimental points. It changes from positive near the z-axis to negative at larger azimuth angles,

https://doi.org/10.1017/jfm.2025.10219 Published online by Cambridge University Press

reaching zero at approximately 21°, consistent with figure 3(*b*). The physics is explained as follows: at small azimuth angles, viscous momentum exchange is predominant, where liquid elements decelerate and transfer momentum to larger angles, thereby increasing thickness. The radial viscous force increases with the azimuth angle, thereby producing a torque that drives rotation from larger to smaller azimuth angles. Significant angular velocity u_ϕ at large azimuth angles drives mass transport from larger to smaller angles, resulting in a rapid decrease in thickness. Figure 4(*c*) shows the momentum exchange contribution to $a(\phi)$ as the solid line; the remaining portion represents angular mass transport.

Figure 4(*d–f*) compares the measured fringes with theoretical predictions from our thickness model and the H&P model for a mixture with $\nu = 18.0$. Our model closely matches experimental results; conversely, the H&P model exhibits significant discrepancies in both fringe orders and spatial distribution. Figure 4(*g*) illustrates the relative deviation of our model from the H&P model. While the experimental results show nearly perfect consistency with our model, they deviate from the H&P model by a factor of 0.4–1.6. The extent of viscous effects is determined by the maximum value that r can take, and figure 4(*h*) shows the liquid sheet length L, which can be fitted as $L/R_j \propto WeRe^{0.2}$. Overall, regulating viscosity and surface tension offers precise in situ control over liquid-sheet size and thickness, overcoming current limitations that rely on mechanical regulation, particularly in microfluidic chips (Loh *et al.* 2020; Treffert *et al.* 2022). This can be achieved by adjusting solution components and solute or, for magnetorheological fluids, by applying a magnetic field (Du *et al.* 2024).

The viscous effects are significant when the Ohnesorge number in the sheet is comparable to 1: $Oh = \nu(h\sigma/\rho)^{-1/2} \sim 1$. In this work, $Oh \sim 10-100$, but for large-scale, low-speed liquid systems with $R_j > 1$ mm, the viscous effects are weak as $Oh \ll 1$. Considering $h \propto R_j^2$, $Q = \pi u_j R_j^2$, $u_j R_j \sim$ const., we can estimate that $\delta \propto Q^{-1} \propto Oh$. For this reason, the H&P model, in which thickness is considered independent of ν and Q, has been adequate for many years due to the relatively large flow rate. However, with the increasing importance of microscale, ultra-thin liquid sheets, viscous effects must now be taken into consideration. Moreover, the momentum exchange and mass transport are fundamental aspects for the further understanding of liquid sheets, including those formed by converging (Crissman *et al.* 2022) and gas-assisted nozzles, as the underlying physics is similar (Woo *et al.* 2018).

3. Conclusions

In conclusion, our study demonstrates the critical role of viscosity in determining the thickness distribution of microscale impinging liquid sheets, while surface tension primarily governs their shape. Viscosity-induced effects substantially broaden the accessible thickness range and accelerate thickness changes. The proposed model, based on momentum exchange and mass transport dynamics, accurately predicts viscous effects previously overlooked in classical theories. These findings enable precise control of sheet thickness, which is crucial for applications such as laser-driven ion acceleration where ultra-thin targets are required. By implementing the method described in this work, we anticipate generating sub-50 nm sheets, which will unlock a range of new physical phenomena (Peng *et al.* 2024). Furthermore, independent control of the liquid sheet's shape and thickness facilitates improved nozzle atomization and chemical reactor control. Such strategies based on model predictions should open up new possibilities across various applications.

https://doi.org/10.1017/jfm.2025.10219 Published online by Cambridge University Press

Supplementary material. Supplementary material is available at https://doi.org/10.1017/jfm.2025.10219.

Funding. The work has been supported by the National Grand Instrument Project (grant no. 2019YFF01014402), the National Science Fund for Distinguished Young Scholars (12225501), the Guangdong High-level Innovation Research Institute (2021B0909050006), the National Natural Science Foundation (grant nos 12205008, U23B6009 and 12272050), the National Key Research and Development Program of China (grant no. 2024YFF0726304), the Beijing Natural Science Foundation (grant no.1252019).

Declaration of interests. The authors report no conflicts of interest.

Author contributions. Z.Y.P. designed the experiments and developed the theoretical framework; X.L. performed the experiments and analysed the data; Z.Y.S. formulated key hypotheses and derived the relevant equations; B.W., E.J.W. and X.D.C. conducted the simulations and provided helpful discussions; Z.X.C., J.R.Z. and Y.G. contributed to the experimental foundation; W.J.M. provided guidance on the core physics concepts and directed the article structure.

Data availability statement. The data supporting this study's findings are available from the corresponding author upon reasonable request.

References

Baber, R., Mazzei, L., Thanh, N.T.K. & Gavriilidis, A. 2016 Synthesis of silver nanoparticles using a microfluidic impinging jet reactor. *J. Flow Chem.* **6** (3), 268–278.

Bremond, N. & Villermaux, E. 2006 Atomization by jet impact. *J. Fluid Mech.* **549** (-1), 273–306.

Bush, J.W.M. & Hasha, A.E. 2004 On the collision of laminar jets: fluid chains and fishbones. *J. Fluid Mech.* **511**, 285–310.

Buttersack, T., Haak, H., Bluhm, H., Hergenhahn, U., Meijer, G. & Winter, B. 2023 Imaging temperature and thickness of thin planar liquid water jets in vacuum. *Struct. Dyn.-US* **10** (3).

Chen, M., Pukhov, A., Yu, T.P. & Sheng, Z.M. 2009 Enhanced collimated gev monoenergetic ion acceleration from a shaped foil target irradiated by a circularly polarized laser pulse. *Phys. Rev. Lett.* **103** (2), 024801.

Choo, Y.J. & Kang, B.S. 2001 Parametric study on impinging-jet liquid sheet thickness distribution using an interferometric method. *Exp. Fluids* **31** (1), 56–62.

Choo, Y.J. & Kang, B.S. 2007 The effect of jet velocity profile on the characteristics of thickness and velocity of the liquid sheet formed by two impinging jets. *Phys. Fluids* **19** (11).

Choo, Y.-J. & Kang, B.-S. 2002 The velocity distribution of the liquid sheet formed by two low-speed impinging jets. *Phys. Fluids* **14** (2), 622–627.

Crissman, C.J., 2022 Sub-micron thick liquid sheets produced by isotropically etched glass nozzles. *Lab Chip* **22** (7), 1365–1373.

Du, T., Zhao, P., Liu, Y., Ma, N., Dong, X. & Huang, H. 2024 Balanced devil triangle: a satisfactory comprehensive performance magnetorheological fluids with cross-scale particles. *Adv. Funct. Mater.* **34** (4), 2311254.

Ekimova, M., Quevedo, W., Faubel, M., Wernet, P. & Nibbering, E.T.J. 2015 A liquid flatjet system for solution phase soft-x-ray spectroscopy. *Struct. Dyn.-US* **2** (5).

Füle, M., Kovács, A.P., Gilinger, T., Karnok, M., Gaál, P., Figul, S., Marowsky, G. & Osvay, K. 2024 Development of an ultrathin liquid sheet target for laser ion acceleration at high repetition rates in the kilohertz range. *High Power Laser Sci. Engng* **12**, e37.

Hasson, D. & Peck, R.E. 1964 Thickness distribution in a sheet formed by impinging jets. *AIChE J.* **10** (5), 752–754.

Ibrahim, E.A. & Przekwas, A.J. 1991 Impinging jets atomization. *Phys. Fluids A: Fluid Dyn.* **3** (12), 2981–2987.

Kim, Y.H. 2023 High-harmonic generation from a flat liquid-sheet plasma mirror. *Nat. Commun.* **14** (1), 2328.

Knight, B.M. 2024 Detailed characterization of kHz-rate laser-driven fusion at a thin liquid sheet with a neutron detection suite. *High Power Laser Sci. Engng* **12**, e2.

Li, R. & Ashgriz, N. 2006 Characteristics of liquid sheets formed by two impinging jets. *Phys. Fluids* **18** (8).

Loh, Z.-H. 2020 Observation of the fastest chemical processes in the radiolysis of water. *Science* **367** (6474), 179–182.

Lu, J. & Corvalan, C.M. 2014 Influence of viscosity on the impingement of laminar liquid jets. *Chem. Engng Sci.* **119**, 182–186.

https://doi.org/10.1017/jfm.2025.10219 Published online by Cambridge University Press

MACCHI, A., BORGHESI, M. & PASSONI, M. 2013 Ion acceleration by superintense laser-plasma interaction. *Rev. Mod. Phys.* **85** (2), 751–793.
MAJUMDAR, N. & TIRUMKUDULU, M.S. 2018 Dynamics of radially expanding liquid sheets. *Phys. Rev. Lett.* **120** (16), 164501.
MORRISON, J.T., FEISTER, S., FRISCHE, K.D., AUSTIN, D.R., NGIRMANG, G.K., MURPHY, N.R., ORBAN, C., CHOWDHURY, E.A. & ROQUEMORE, W.M. 2018 MeV proton acceleration at kHz repetition rate from ultra-intense laser liquid interaction. *New J. Phys.* **20** (2), 022001.
OEFELEIN, J.C. & YANG, V. 1993 Comprehensive review of liquid-propellant combustion instabilities in F-1 engines. *J. Propul. Power* **9** (5), 657–677.
PANAO, M.R.O. & DELGADO, J.M.D. 2013 Effect of pre-impingement length and misalignment in the hydrodynamics of multijet impingement atomization. *Phys. Fluids* **25** (1).
PENG, Z. *et al.* 2024 A comprehensive diagnostic system of ultra-thin liquid sheet targets. *High Power Laser Sci.Engng* **12**, e26.
SANJAY, V. & DAS, A.K. 2017 Formation of liquid chain by collision of two laminar jets. *Phys. Fluids* **29** (11).
SAVART, F. 1833 Mémoire sur le choc de deux veines liquides animées de mouvements directement opposés. *Ann. Chim. Phys.* **54**, 257–310.
STEMER, D. *et al.* 2023 Photoelectron spectroscopy from a liquid flatjet. *J. Chem. Phys.* **158** (23).
STREETER, M.J.V. 2025 Stable laser-acceleration of high-flux proton beams with plasma collimation. *Nat. Commun.* **16** (1), 1004.
TAYLOR, G. 1961 Formation of thin flat sheets of water. *Proc. R. Soci. Lond. Series A. Math. Phys. Sci.* **259** (1296), 1–17.
TCYPKIN, A.N., PONOMAREVA, E.A., PUTILIN, S.E., SMIRNOV, S.V., SHTUMPF, S.A., MELNIK, M.V., E, Y., KOZLOV, S.A. & ZHANG, X.-C. 2019 Flat liquid jet as a highly efficient source of terahertz radiation. *Opt. Express* **27** (11), 15485–15494.
TREFFERT, F. *et al.* 2022 High-repetition-rate, multi-MeV deuteron acceleration from converging heavy water microjets at laser intensities of 1021 W/cm2. *Appl. Phys. Lett.* **121** (7).
VISSER, C.W., KAMPERMAN, T., KARBAAT, L.P., LOHSE, D. & KARPERIEN, M. 2018 In-air microfluidics enables rapid fabrication of emulsions, suspensions, and 3D modular (bio)materials. *Sci. Adv.* **4** (1), eaao1175.
WOO, S. *et al.* 2018 Current-driven dynamics and inhibition of the skyrmion Hall effect of ferrimagnetic skyrmions in GdFeCo films. *Nat. Commun.* **9** (1), 959.
XIAODONG, C. & VIGOR, Y. 2019 Recent advances in physical understanding and quantitative prediction of impinging-jet dynamics and atomization. *Chinese J. Aeronaut.* **32** (1), 45–57.
YANG, J. *et al.* 2021 Direct observation of ultrafast hydrogen bond strengthening in liquid water. *Nature* **596** (7873), 531–535.
YANG, L.-J., ZHAO, F., FU, Q.-F. & CUI, K.-D. 2014 Liquid sheet formed by impingement of two viscous jets. *J. Propul. Power* **30** (4), 1016–1026.
ZHANG, C., ZHANG, Z., WU, K., XIA, X. & FAN, X. 2021 Atomization of misaligned impinging liquid jets. *Phys. Fluids* **33** (9).
ZIEGLER, T. *et al.* 2024 Laser-driven high-energy proton beams from cascaded acceleration regimes. *Nat. Phys.* **20** (7), 1211–1216.

https://doi.org/10.1017/jfm.2025.10219 Published online by Cambridge University Press